

Near-threshold  $\pi^-$  photoproduction on the deuteron

B. Strandberg,<sup>1,\*</sup> K. G. Fissum,<sup>2,†</sup> J. R. M. Annand,<sup>1</sup> W. J. Briscoe,<sup>3</sup> J. Brudvik,<sup>4</sup> F. Cividini,<sup>5</sup>  
 L. Clark,<sup>1</sup> E. J. Downie,<sup>3</sup> K. England,<sup>6</sup> G. Feldman,<sup>3</sup> D. I. Glazier,<sup>1</sup> K. Hamilton,<sup>1</sup> K. Hansen,<sup>4</sup>  
 L. Isaksson,<sup>4</sup> R. Al Jebali,<sup>1</sup> M. A. Kovash,<sup>7</sup> A. E. Kudryavtsev,<sup>3,8</sup> V. Lensky,<sup>9</sup> S. Lipschutz,<sup>3</sup> M. Lundin,<sup>4</sup>  
 M. Meshkian,<sup>2</sup> D. G. Middleton,<sup>5,10</sup> L. S. Myers,<sup>11</sup> D. O'Donnell,<sup>1</sup> G. V. O'Rielly,<sup>12</sup> B. Oussena,<sup>3</sup>  
 M. F. Preston,<sup>2</sup> B. Schröder,<sup>2,4</sup> B. Seitz,<sup>1</sup> I. I. Strakovsky,<sup>3</sup> M. Taragin,<sup>3</sup> and V. E. Tarasov<sup>8</sup>

(The PIONS@MAX-lab Collaboration)

<sup>1</sup>*School of Physics and Astronomy, University of Glasgow, Glasgow G12 8QQ, Scotland UK*

<sup>2</sup>*Department of Physics, Lund University, SE-221 00 Lund, Sweden*

<sup>3</sup>*Institute for Nuclear Studies, Department of Physics,*

*The George Washington University, Washington DC 20052, USA*

<sup>4</sup>*MAX IV Laboratory, Lund University, SE-221 00 Lund, Sweden*

<sup>5</sup>*Institut für Kernphysik, Johannes Gutenberg-Universität Mainz, D-55099 Mainz, Germany*

<sup>6</sup>*College of Engineering, University of Massachusetts Dartmouth, North Dartmouth MA 02747, USA*

<sup>7</sup>*Department of Physics and Astronomy, University of Kentucky, Lexington, KY 40506, USA*

<sup>8</sup>*National Research Centre "Kurchatov Institute",*

*Institute for Theoretical and Experimental Physics (ITEP), Moscow 117218, Russia*

<sup>9</sup>*Institut für Kernphysik & Cluster of Excellence PRISMA,*

*Johannes Gutenberg Universität, Mainz D-55099, Germany*

<sup>10</sup>*Mount Allison University, Sackville, New Brunswick E4L 1E6, Canada.*

<sup>11</sup>*Bluffton University, 1 University Drive, Bluffton, OH 45817, USA*

<sup>12</sup>*Department of Physics, University of Massachusetts Dartmouth, Dartmouth MA 02747, USA*

(Dated: December 10, 2018)

The first experimental investigation of the near-threshold cross section for incoherent  $\pi^-$  photoproduction on the deuteron  $\gamma d \rightarrow \pi^- pp$  is presented. The total cross section has been measured using an unpolarized tagged-photon beam, a liquid-deuterium target, and three large NaI(Tl) spectrometers. The experimental technique involved detection of the  $\sim 131$  MeV gamma ray resulting from the radiative capture of photoproduced  $\pi^-$  in the target. The data are compared to theoretical models that give insight into the elementary reaction  $\gamma n \rightarrow \pi^- p$  and pion-nucleon and nucleon-nucleon final-state interactions.

Keywords: threshold pion photoproduction, final-state interactions, chiral perturbation theory, deuteron, radiative capture

Incoherent pion photoproduction on the deuteron  $\gamma d \rightarrow \pi NN$  provides information on the elementary reaction on the nucleon  $\gamma N \rightarrow \pi N$  and on pion-nucleon ( $\pi N$ ) and nucleon-nucleon ( $NN$ ) final-state interactions (FSI). The near-threshold cross section for the elementary reaction is sensitive to the  $E_{0+}$  amplitude, which has a long history of theoretical studies closely related to measurements of near-threshold pion photoproduction [1]. Partial-wave analysis (PWA) [2] of experimental data sets may be used to obtain values for this and other photoproduction amplitudes. These amplitudes are vital inputs to low-energy descriptions of hadron physics based on dispersion relations [3] or chiral perturbation theory ( $\chi$ PT) [4]. Tagged-photon beams in combination with advances in detector technology have substantially increased the size of the global pion-production data set over the last few decades. However, most of the measurements have focused on the  $\pi^0$  channel [5–8]. While the threshold cross section for  $\pi^+$  photoproduction was established in Ref. [9], none of the  $E_\gamma < 200$  MeV  $\pi^-$  measurements [10–13] have probed the near-threshold region, with the lowest-energy data point at  $\sim 158$  MeV [13], still more than 10 MeV above threshold. This Letter reports

the pioneering measurement of the total cross section for  $\pi^-$  photoproduction on the deuteron in the energy range 147 – 160 MeV.

The experiment was performed at the Tagged-Photon Facility [14] of the MAX IV Laboratory [15] in Sweden. A tagged-photon beam with energies from 140 – 160 MeV, created via the bremsstrahlung-tagging technique [16, 17], was incident on a thin cylindrical Kapton vessel that contained liquid deuterium ( $\text{LD}_2$ ) with density  $\rho_D = (0.163 \pm 0.001)$  g/cm<sup>3</sup>. The tagged-photon energies  $E_\gamma$  were determined by momentum analysis of the post-bremsstrahlung electrons using a dipole magnet together with a 64-channel focal-plane (FP) hodoscope [18]. The tagged-photon energy resolution was  $\pm 0.3$  MeV. Electron arrival times at the hodoscope were digitized with multi-hit (mhit) time-to-digital converters (TDCs). The post-bremsstrahlung recoil electron counting rate (typically 0.1 – 1 MHz per FP channel), necessary for the photon-flux determination, was measured by time-normalized scalars. Tagging efficiency, the fraction of bremsstrahlung photons which passed through the collimation system en route to the target, was measured daily. The mean tagging efficiency was  $(\sim 23 \pm 2^{\text{sys.}})\%$ .

See Ref. [19] for further details describing the beam and target setup.

Three large NaI(Tl) spectrometers [20–22] were placed at laboratory angles  $\theta = 60^\circ$ ,  $120^\circ$  and  $150^\circ$  to detect photons originating from the LD<sub>2</sub> target. Each NaI(Tl) spectrometer consisted of a large cylindrical core crystal surrounded by an annulus of optically isolated crystal segments. The segments were in turn surrounded by plastic scintillators. Scintillation light was read out by photomultiplier tubes (PMTs) attached to the rear faces of the scintillators. Analog signals from the PMTs were recorded by charge-integrating analog-to-digital converters (ADCs).

Data were recorded on an event-by-event basis. The data-acquisition and data-analysis software were based on ROOT [23] and RooFit [24] frameworks. The data acquisition was triggered by an energy deposition greater than  $\sim 50$  MeV in any of the three detectors, which initiated the readout of the ADCs and started the mhit TDCs. The mhit TDC stop signals came from the post-bremsstrahlung recoil electrons striking the FP channels. The ADC information was used to reconstruct detected photon energies, whereas the FP TDC information established the coincidence between the post-bremsstrahlung recoil electrons and the particles detected with the spectrometers. The data were collected over three four-week run periods in June and September 2011 and April 2015.

Each NaI(Tl) detector was calibrated from its in-beam response to a low-intensity tagged-photon beam. Cosmic-ray muons that traversed the detectors during data taking were identified with the annulus scintillators by requiring coincident signals in opposing annular segments. The pulse-height variations of identified cosmic-ray muon events registered by the PMTs were used to correct for PMT gain instabilities [19]. After calibration procedures, the NaI(Tl) detectors had an energy resolution of  $\sim 3$  MeV (full width at half maximum). The absolute calibration of the tagged-photon energies and the NaI(Tl) detectors was determined with an accuracy of  $\pm 0.4$  MeV by reconstructing the 131.4 MeV photon-energy end-point from the radiative-capture (RC) reaction  $\pi^- d \rightarrow \gamma nn$  [25].

Photons from the RC reaction were also used to determine the yield of photoproduced  $\pi^-$ . The near-threshold  $\pi^-$  had low kinetic energies and most were instantaneously captured inside the LD<sub>2</sub> target. The two dominant capture channels are non-radiative capture (NRC)  $\pi^- d \rightarrow nn$  (absolute branching ratio  $BR_{\text{nrc}} = 0.739 \pm 0.010$ ) and the previously mentioned RC ( $BR_{\text{rc}} = 0.261 \pm 0.004$ ) [26]. Using these branching ratios and the energy spectrum of the RC photons [25, 27, 28], the  $\pi^-$  photoproduction yield was obtained. Figure 1 depicts the simulated energy spectra of the dominant background reactions of deuteron photodisintegration ( $np$  sim),  $\pi^0$  photoproduction ( $\pi^0$  sim) and  $\pi^-$  NRC ( $nn$  sim), alongside the theoretical RC spectrum

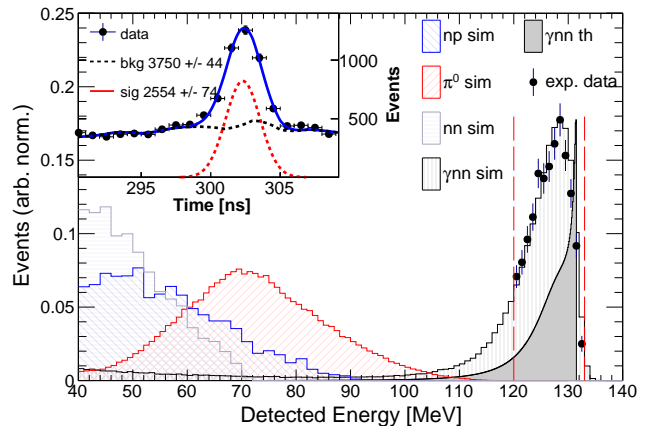


FIG. 1. (Color online) Simulated energy spectra of dominant reaction channels alongside the measured energy spectrum and a theoretical energy spectrum of  $\pi^-$  RC (see text on pp. 2). Inset: A typical fit to a timing-coincidence spectrum for events inside the cut  $E_{\text{det}} \in [120, 133]$  MeV for yield determination.

( $\gamma nn$  th) [27, 29], the simulated RC spectrum ( $\gamma nn$  sim) and the measured energy spectrum (*exp. data*). Simulations were performed with software based on GEANT4 [30]. The photoproduced  $\pi^+$  did not constitute a significant background, as the muons from the dominant subsequent decay  $\pi^+ \rightarrow \mu^+ \nu_\mu$  did not deposit more than  $\sim 50$  MeV in any of the NaI(Tl) detectors. Additionally, the positrons from the decay  $\mu^+ \rightarrow e^+ \nu_e \bar{\nu}_\mu$  were almost always outside the timing coincidence window with respect to the post-bremsstrahlung recoil electron. The simulated RC spectrum was obtained by first matching the Monte Carlo in-beam data to the experimental in-beam data as described in Refs. [19, 31]. Then, photons with energies sampled from the theoretical RC spectrum and an isotropic angular distribution were generated in the LD<sub>2</sub> target into  $4\pi$  solid angle. Energy deposited by the photons in the NaI(Tl) detectors was smeared to account for the previously determined resolution effects, which led to the simulated RC spectrum depicted in Fig. 1. The simulation is in excellent agreement with the data and indicated that the dominant background reactions could be removed by a cut on the detected energy  $E_{\text{det}} \in [120, 133]$  MeV. Background from elastic  $\gamma d \rightarrow \gamma d$  and inelastic  $\gamma d \rightarrow \gamma np$  Compton scattering could not be separated. Contamination from Compton scattering channels was angle- and energy-dependent, but at the present energies, the scattering cross section is only a few percent of the charged-pion photoproduction cross section. The cross-section data from Refs. [19, 32] were extrapolated to produce conservative scattering-contamination estimates. These indicated that the effect on the extracted  $\pi^-$  cross section was typically  $\pm 3\%$  (maximum of 5.5% at lowest  $E_\gamma$ ). This effect was accounted for in the systematic uncer-

tainty analysis discussed below.

The total cross section for  $\pi^-$  photoproduction on the deuteron was determined according to

$$\sigma = \frac{Y4\pi}{\Omega_{\text{eff}}N_{\gamma}\kappa_{\text{eff}}P_cBR_{\text{rc}}}. \quad (1)$$

In Eq. (1),  $Y$  is the yield of RC photons,  $\Omega_{\text{eff}}$  is the detector acceptance,  $N_{\gamma}$  is the tagged-photon flux incident on the target,  $\kappa_{\text{eff}}$  is the effective target thickness,  $P_c$  is the  $\pi^-$  capture probability inside the LD<sub>2</sub> target and  $BR_{\text{rc}}$  is the absolute branching ratio for RC. The factor  $4\pi$  in the numerator originates from the assumption that the photons from RC are emitted isotropically. For the determination of the yield, for each detector, timing-coincidence spectra with respect to the post-bremsstrahlung recoil electrons were filled for events inside the cut  $E_{\text{det}} \in [120, 133]$  MeV. The FP channels were grouped in eight  $\sim 2.5$  MeV wide bins, resulting in eight spectra per detector. The resulting spectra had a coincidence peak superimposed upon events that were in random coincidence. As the dominant background reactions were removed by the cut on  $E_{\text{det}}$ ,  $\pi^-$  capture yields could be determined directly from fits to the coincidence spectra, as illustrated in the inset of Fig. 1. The signal peak was represented by a Gaussian. The background from random coincidences had a time structure due to a time modulation of the electron-beam intensity related to the pulse-stretching and beam-extraction apparatus [33]. The first two FP energy bins were below  $\pi^-/\pi^+$  threshold. Thus, the coincidence spectra for these bins were completely dominated by random coincidences, which allowed estimation of the random-background shape. The fit was moderately dependent on the width of the fitted window around the coincidence peak, which led to a systematic uncertainty of  $\sim 2\%$  (7% at lowest  $E_{\gamma}$ ). Systematic uncertainty due to contamination from  $\pi^-$  produced in the thin-walled Kapton vessel was estimated to be  $\sim 1.5\%$  by taking into account the chemical composition of Kapton, the thickness of the endcaps of the vessel and assuming that the  $\pi^-$  photoproduction cross section on  $^{12}\text{C}$  and  $^{16}\text{O}$  scales linearly with the number of neutrons per atom.

The detector acceptance  $\Omega_{\text{eff}}$  was determined from the GEANT4-simulated RC spectrum described previously. The detector acceptance was determined by

$$\Omega_{\text{eff}} = 4\pi N_{E_{\text{det}} \in [120, 133] \text{ MeV}} / N_{\text{tot}}. \quad (2)$$

In Eq. (2),  $N_{\text{tot}}$  is the total number of Monte-Carlo photons simulated inside the target, with energies sampled from the theoretical RC spectrum and directions sampled from a phase-space distribution over  $4\pi$  solid angle. The numerator is the number of events in a detector within the energy cut  $E_{\text{det}} \in [120, 133]$  MeV. The acceptances of the detectors at  $60^\circ$ ,  $120^\circ$  and  $150^\circ$  were  $\sim 46$  msr,  $\sim 30$  msr and  $\sim 26$  msr, respectively. The dominant systematic uncertainty of 5% originated from the

uncertainty in the theoretical model for RC [29]. Systematic uncertainty from the positioning accuracy of the detectors and the target was estimated to be  $\sim 3\%$  by varying the detector and target positions in the simulation within realistic limits. The  $\pm 0.4$  MeV uncertainty in the overall energy calibration of the detectors was propagated into the acceptance calculation and was estimated to have an effect of  $\sim 1.5\%$  by varying the energy cut by the uncertainty in the simulation and recording the effect on the acceptance.

The tagged-photon flux  $N_{\gamma}$  was established by multiplying the counts in the FP hodoscope channels by the measured tagging efficiencies ( $\sim 2\%$  systematic uncertainty from tagging efficiency). The effective target thickness was

$$\kappa_{\text{eff}} = (8.14 \pm 0.10) \cdot 10^{23} \text{ nuclei/cm}^2, \quad (3)$$

with a  $\sim 1.2\%$  systematic uncertainty originating from the geometry of the target. Further details about  $N_{\gamma}$  and  $\kappa_{\text{eff}}$  can be found in Ref. [19].

The capture probability of photoproduced  $\pi^-$  was estimated from a GEANT4 simulation, where  $\pi^-$  were simulated inside the LD<sub>2</sub> target. The X-Y coordinates of the vertices were sampled from a simulated intensity distribution of the photon beam determined by the geometry of the beam line, and the Z-coordinates (along the beam axis) were distributed uniformly over the length of the target. In sampling the momenta of the  $\pi^-$ , the Fermi momentum of the bound neutron in the deuteron [34], the energy of the incident photon and the  $\cos\theta_{\text{cm}}$  distribution of the pions in the elementary photoproduction reaction [35] were taken into account. The dominant systematic uncertainty of  $\lesssim 3.1\%$  originated from the  $\pm 0.4$  MeV uncertainty in the tagged-photon energies. Uncertainty due to the simulation of the beam profile was estimated to be  $\lesssim 1.6\%$  by changing the beam radius by  $\pm 10\%$  in

quantity	source	magnitude	in std. dev.
$Y$	fit	2%–7%	✓
	scattering	$\lesssim 5.5\%$	✓
	Kapton	1.5%	
$\Omega_{\text{eff}}$	positioning	3%	✓
	$E_{\text{cut}}$	1.5%	✓
	model $_{\gamma 2n}$	5%	
$N_{\gamma}$	tagg. eff.	2%	✓
$\kappa_{\text{eff}}$	geometry	1.2%	
$P_c$	beam sim.	$\lesssim 1.6\%$	
	$\Delta E_{\gamma}$	$\lesssim 3.1\%$	
$BR_{\text{rc}}$	measurement	1.5%	

TABLE I. Summary of the dominant systematic uncertainties. The right column indicates whether or not the systematic uncertainty is considered to contribute to the standard deviation of the nine cross-section measurements.

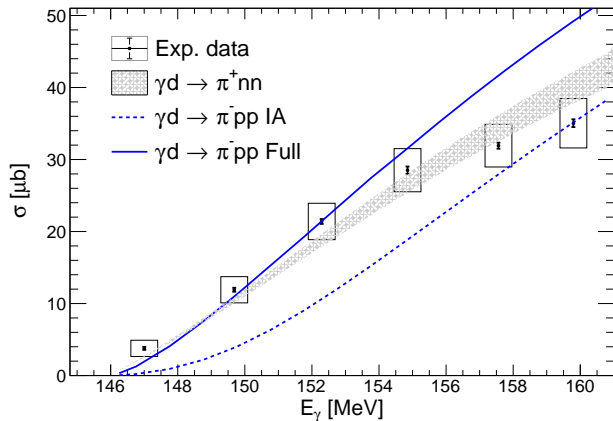


FIG. 2. (Color online) Measured total cross section for  $\pi^-$  photoproduction on the deuteron with statistical (error bars) and systematic (error boxes) uncertainties alongside theoretical predictions for  $\gamma d \rightarrow \pi^+ nn$  (gray band) [37] and  $\gamma d \rightarrow \pi^- pp$  in the Impulse Approximation (blue dashed line) and with FSI (blue solid line) [38].

the simulation and recording the effect on  $P_c$ . The radius of the actual beam spot  $r_{\text{beam}} \sim 20$  mm (estimated both from simulation and a photograph of the beam at the target location) was substantially smaller than the radius of the Kapton vessel  $r_{\text{vessel}} = 34$  mm. Additionally, the  $\pi^-$  escape from the target occurred predominantly from the downstream endcap, which explains the relatively weak dependence on the radius of the beam.

The reported cross section for threshold  $\pi^-$  photoproduction at each energy was determined as a statistically weighted average of nine measurements (three detectors and three run periods). The standard deviation of the nine measurements was used to estimate the combined systematic uncertainty. Various sources of systematic uncertainties described in this Letter are summarized in Table I. The right column of Table I specifies whether or not a given systematic uncertainty was considered to contribute to the standard deviation of the nine measurements. Typically, the uncertainty estimated from the standard deviation was of similar magnitude or slightly larger compared to the uncertainty estimated from adding the contributing sources in quadrature. The sources of systematic uncertainty that did not contribute to the standard deviation were added to it in quadrature to arrive at the systematic uncertainties quoted in Table II and shown in Fig. 2. Of the uncertainties that did not contribute to the standard deviation, only the capture efficiency could affect the shape of the cross-section curve. Others could affect only the scale of the results. The angle- and energy-dependent uncertainties from scattering channels are accounted for in the standard deviation. A full account of the analysis of the experimental data is available in [36].

$E_\gamma$ [MeV]	$\sigma \pm \text{err}_{\text{stat.}} \pm \text{err}_{\text{sys.}}$ [ $\mu\text{b}$ ]
147.0	$3.8 \pm 0.2$ (5.3%) $\pm 1.1$ (28.9%)
149.7	$11.9 \pm 0.3$ (2.5%) $\pm 1.8$ (15.1%)
152.3	$21.4 \pm 0.3$ (1.4%) $\pm 2.5$ (11.7%)
154.9	$28.5 \pm 0.5$ (1.8%) $\pm 3.0$ (10.5%)
157.6	$31.9 \pm 0.4$ (1.3%) $\pm 3.0$ (9.4%)
159.8	$35.0 \pm 0.5$ (1.4%) $\pm 3.4$ (9.7%)

TABLE II. Measured total cross section for  $\pi^-$  photoproduction on the deuteron with statistical and systematic uncertainties.

The experimental data for the  $\gamma d \rightarrow \pi^- pp$  reaction are now compared with model predictions. The additional final-state proton compared to the elementary reaction  $\gamma n \rightarrow \pi^- p$  introduces additional FSI that have a non-negligible effect on the cross section and need to be taken into account. The first model [38] is calculated from the four diagrams in Fig. 3, where  $M_a$  is the Impulse Approximation (IA) term,  $M_b$  and  $M_c$  are the  $NN$  and  $\pi N$  FSI terms, and  $M_d$  is the  $NN$ -FSI term with pion rescattering in the intermediate state (referred to as the ‘two-loop’ term). The ingredients and the approximations for the computation of the four terms are discussed in the points below.

1) The elementary reaction is described by the  $s$ -wave amplitude, which is determined by the  $E_{0+}$  multipole. The value of the  $E_{0+}$  multipole as extracted by various analyses has been very stable over the last decades and here  $E_{0+} = -31.9$  from Ref. [1] is used. The  $E_{0+}$  amplitude is expressed in the conventional units of  $10^{-3}/m_{\pi^+}$ , which is assumed throughout this Letter. Further, in diagrams  $M_c$  and  $M_d$ , only charged intermediate pions are included as the neutral-pion photoproduction amplitude is much smaller than the charged-pion photoproduction amplitude in the near-threshold region. In this approxi-

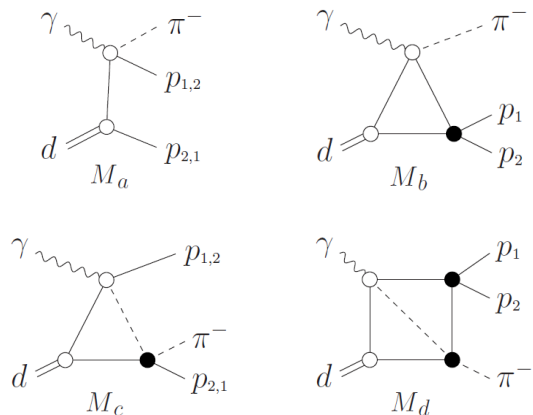


FIG. 3. IA ( $M_a$ ),  $NN$ -FSI ( $M_b$ ),  $\pi N$ -FSI ( $M_c$ ) and two-loop ( $M_d$ ) diagram for  $\gamma d \rightarrow \pi^- pp$ . Filled black circles indicate FSI vertices.

mation, the cross section is proportional to  $|E_{0+}|^2$ .

2) The  $s$ -wave  $pp$ -scattering amplitude includes Coulomb effects and is taken in the Effective-Range Approximation [37], using the values  $a_{pp} = -7.8$  fm for the  $pp$  scattering length and  $r_{pp} = 2.8$  fm for the effective range. Off-shell effects are included as in Refs. [38, 39].

3) For  $\pi N$  scattering, the  $s$ -wave  $\pi N$  amplitude  $f_{\pi^- p} = b_0 - b_1$  is used, fixed by the isospin scattering lengths  $b_0 = -28$  and  $b_1 = -881$  in units  $10^{-4}/m_\pi$  [40].

4) The deuteron wave function (DWF) derived from the Bonn potential is used in parameterized form from Ref. [41]. The IA diagram  $M_a$  includes both the  $s$ -wave and the  $d$ -wave part of the DWF, with the  $d$ -wave having only a small effect on the cross section at energies close to threshold. The inclusion of the  $d$ -wave part of the DWF in other diagrams is expected to have a negligible effect on the cross section and is excluded to simplify calculations.

The cross-section model is depicted alongside the experimental data in Fig. 2. The dashed curve indicates the IA that corresponds to diagram  $M_a$ , whereas the solid curve indicates the full model as calculated from the four diagrams in Fig. 3. The dominant correction to the IA term  $M_a$  originates from the  $NN$ -FSI amplitude  $M_b$ , whereas the combined contribution from the  $\pi N$ -FSI ( $M_c$ ) and the two-loop term ( $M_d$ ) is typically  $\lesssim 10\%$ . While the model and the experimental data agree within uncertainties in the energy region 147 – 157 MeV, the model noticeably overestimates the data above 157 MeV. This is caused by two dominant factors. First, the model does not account for the energy dependence of the  $E_{0+}$  multipole. Since  $E_{0+}$  decreases with energy, this approximation causes the theoretical model to overestimate the cross section as  $E_\gamma$  increases from threshold. Second, the model uses only the  $s$ -wave amplitude for the elementary reaction  $\gamma n \rightarrow \pi^- p$  and for  $NN$ -FSI, which is a likely contributor to the divergence and indicates that higher partial waves may have a significant effect for energies  $\gtrsim 10$  MeV above threshold.

The measured cross section for  $\gamma d \rightarrow \pi^- pp$  is also compared to an existing theoretical  $\chi$ PT prediction for the isospin-partner channel  $\gamma d \rightarrow \pi^+ nn$  [37]. Comparison of the  $\pi^-$  experimental data with the  $\pi^+$  prediction is insightful, as the  $\chi$ PT calculation uses higher-order partial waves both for the elementary reaction  $\gamma p \rightarrow \pi^+ n$  and for the  $NN$ -FSI compared to the model from Ref. [38]. It also accounts for the energy dependence of the  $E_{0+}$  multipole. In the leading order of the chiral expansion, the elementary amplitudes  $\gamma n \rightarrow \pi^- p$  and  $\gamma p \rightarrow \pi^+ n$  are equal. The most important difference between the elementary  $\pi^+$  and  $\pi^-$  photoproduction reactions is the proton recoil in the latter, which increases the dipole moment of the final  $\pi N$  system. Due to the absence of proton recoil in the  $\pi^+$  reaction, the absolute value of the  $E_{0+}$  amplitude is approximately 12% smaller for  $\gamma p \rightarrow \pi^+ n$  compared

to  $\gamma n \rightarrow \pi^- p$  and for this calculation  $E_{0+} = 28.2$  from Ref. [42] was used. This effect suppresses the cross section for  $\gamma d \rightarrow \pi^+ nn$  compared to  $\gamma d \rightarrow \pi^- pp$ . On the other hand, there is no Coulomb FSI in  $\pi^+$  photoproduction on the deuteron, which leads to a relative increase in the cross section compared to  $\gamma d \rightarrow \pi^- pp$ . These two dominant differences between the isospin-partner channels are expected to partially cancel each other. The  $\chi$ PT calculation for  $\gamma d \rightarrow \pi^+ nn$  with theoretical uncertainties (see Ref. [37] for a detailed overview of the uncertainty calculation) is depicted as a gray band in Fig. 2. The start of the theoretical curve has been shifted to 145.8 MeV to account for the difference in the reaction threshold compared to the  $\pi^-$  channel. The calculation has been performed at the order  $\chi^{5/2}$  with respect to the chiral expansion parameter  $\chi = m_\pi/m_N$ , where  $m_\pi$  ( $m_N$ ) stands for the generic pion (nucleon) mass. The experimental data and the  $\gamma d \rightarrow \pi^+ nn$  model agree within uncertainties, which suggests that the differences between the  $\pi^+$  and  $\pi^-$  channels indeed tend largely to cancel. The good agreement between the models and the experimental data at energies  $E_\gamma < 157$  MeV suggests that in the immediate vicinity of the threshold, the dominant processes that contribute to the cross section are relatively well understood. Further insight into the discrepancies between experimental data and the models at energies  $\gtrsim 10$  MeV above threshold could be gained from differential cross-section measurements for  $\gamma d \rightarrow \pi^- pp$ , as they would allow for a more detailed study of the effects of various partial waves.

In summary, the first measurement of the near-threshold cross section for  $\pi^-$  photoproduction on the deuteron has been presented along with model predictions. The models and the experimental data are in good agreement in the vicinity of the threshold and provide new insight into the FSI behavior in this energy regime. An extended article that provides further details about the experiment and the theoretical interpretation is currently in preparation.

The authors would like to thank W. R. Gibbs, B. F. Gibson and G. F. de Téramond for constructive discussions. The authors acknowledge support from the staff of the MAX IV Laboratory. This research has been supported by the Swedish Research Council (Contracts No. 40324901 and No. 80410001), the Crafoord Foundation (Grant No. 20060749), the Scottish Universities Physics Alliance (SUPA), the SUPA Prize Studentship, UK Science and Technology Facilities Council Grants No. 57071/1 and No. 50727/1, US NSF Grant No. PHY1309130, US DOE Grants No. DE-SC0016581, No. DE-SC0016583 and No. DE-FG02-06ER41422, the NFS/IRES Award No. 0553467, RFBR Grant No. 16-02-00767 and the Deutsche Forschungsgemeinschaft (DFG) through the Collaborative Research Center, SFB 1044.

- 
- \* Present address: Nikhef, Science Park 105, 1098 XG Amsterdam, Netherlands
- † Corresponding author; [kevin.fissum@nuclear.lu.se](mailto:kevin.fissum@nuclear.lu.se)
- [1] D. Drechsel and L. Tiator, *J. Phys. G* **18**, 449 (1992), and references therein.
- [2] R. A. Arndt, R. L. Workman, Z. Li, and L. D. Roper, *Phys. Rev. C* **42**, 1853 (1990).
- [3] D. Drechsel, B. Pasquini, and L. Tiator, *Few-Body Syst.* **41**, 13 (2007).
- [4] M. Hilt, B. C. Lehnhart, S. Scherer, and L. Tiator, *Phys. Rev. C* **88**, 055207 (2013).
- [5] J. C. Bergstrom, J. M. Vogt, R. Igarashi, K. J. Keeter, E. L. Hallin, G. A. Retzlaff, D. M. Skopik, and E. C. Booth, *Phys. Rev. C* **53**, 1052 (1996).
- [6] J. C. Bergstrom, R. Igarashi, and J. M. Vogt, *Phys. Rev. C* **55**, 2016 (1997).
- [7] J. C. Bergstrom, *Phys. Rev. C* **58**, 2574 (1998).
- [8] D. Hornidge, P. Aguar Bartolomé, J. R. M. Annand, H. J. Arends, R. Beck, V. Bekrenev, H. Berghäuser, A. M. Bernstein, A. Braghieri, W. J. Briscoe, S. Cherepnaya, M. Dieterle, E. J. Downie, P. Drexler, C. Fernández-Ramírez, L. V. Filkov, D. I. Glazier, P. Hall Barrientos, E. Heid, M. Hilt, I. Jaegle, O. Jahn, T. C. Jude, V. L. Kashevarov, I. Keshelashvili, R. Kondratiev, M. Korolija, A. Koulbardis, D. Krambrich, S. Kruglov, B. Krusche, A. T. Laffoley, V. Lisin, K. Livingston, I. J. D. MacGregor, J. Mancell, D. M. Manley, E. F. McNicoll, D. Mekterovic, V. Metag, S. Micanovic, D. G. Middleton, K. W. Moores, A. Mushkarenkov, B. M. K. Nefkens, M. Oberle, M. Ostrick, P. B. Otte, B. Oussena, P. Pedroni, F. Pheron, A. Polonski, S. Prakhov, J. Robinson, T. Rostomyan, S. Scherer, S. Schumann, M. H. Sikora, A. Starostin, I. Supek, M. Thiel, A. Thomas, L. Tiator, M. Unverzagt, D. P. Watts, D. Werthmüller, and L. Witthauer (A2 Collaboration and CB-TAPS Collaboration), *Phys. Rev. Lett.* **111**, 062004 (2013).
- [9] E. C. Booth, B. Chasan, J. Comuzzi, and P. Bosted, *Phys. Rev. C* **20**, 1217 (1979).
- [10] V. Rossi, A. Piazza, G. Susinno, F. Carbonara, G. Gialanella, M. Napolitano, R. Rinzivillo, L. Votano, G. C. Mantovani, A. Piazzoli, and E. Lodi-Rizzini, *Nuovo Cimento A* **13**, 59 (1973).
- [11] M. Salomon, D. Measday, J.-M. Poutissou, and B. Robertson, *Nucl. Phys. A* **414**, 493 (1984).
- [12] M. Wang, Ph.D. thesis, University Of Kentucky (1992).
- [13] K. Liu, Ph.D. thesis, University Of Kentucky (1994).
- [14] J.-O. Adler, M. Boland, J. Brudvik, K. Fissum, K. Hansen, L. Isaksson, P. Lilja, L.-J. Lindgren, M. Lundin, B. Nilsson, D. Pugachov, A. Sandell, B. Schröder, V. Avdeichikov, P. Golubev, B. Jakobsen, J.R.M. Annand, K. Livingston, R. Igarashi, L. Myers, A. Nathan, W.J. Briscoe, G. Feldman, M. Kovash, D. Branford, K. Föhl, P. Grabmayr, V. Takau, G. O’Rielly, D. Burdeynyi, V. Ganenko, V. Morochovskiy, and G. Vashchenko, *Nucl. Instrum. Methods Phys. Res. Sect. A* **715**, 1 (2013).
- [15] M. Eriksson, in *Proceedings of IPAC, Dresden, Germany* (2014).
- [16] J.-O. Adler, B.-E. Andersson, K. I. Blomqvist, B. Forkman, K. Hansen, L. Isaksson, K. Lindgren, D. Nilsson, A. Sandell, B. Schröder, and K. Ziakas, *Nucl. Instrum. Methods Phys. Res. Sect. A* **294**, 15 (1990).
- [17] J.-O. Adler, B.-E. Andersson, K. I. Blomqvist, K. G. Fissum, K. Hansen, L. Isaksson, B. Nilsson, D. Nilsson, H. Ruijter, A. Sandell, B. Schröder, and D. A. Sims, *Nucl. Instrum. Methods Phys. Res. Sect. A* **388**, 17 (1997).
- [18] J. M. Vogt, R. E. Pywell, D. M. Skopik, E. L. Hallin, J. C. Bergstrom, H. S. Caplan, K. I. Blomqvist, W. D. Bianco, and J. W. Jury, *Nucl. Instrum. Methods Phys. Res. Sect. A* **324**, 198 (1993).
- [19] B. Strandberg, J. R. M. Annand, W. Briscoe, J. Brudvik, F. Cividini, L. Clark, E. J. Downie, K. England, G. Feldman, K. G. Fissum, D. I. Glazier, K. Hamilton, K. Hansen, L. Isaksson, R. A. Jebali, M. A. Kovash, S. Lipschutz, M. Lundin, M. Meshkian, D. G. Middleton, L. S. Myers, D. O’Donnell, G. O’Rielly, B. Oussena, M. F. Preston, B. Schröder, B. Seitz, I. Strakovsky, and M. Taragin (The COMPTON@MAX-lab Collaboration), *Phys. Rev. C* **98**, 012201 (2018).
- [20] A. Hüniger, J. Peise, A. Robbiano, J. Ahrens, I. Anthony, H.-J. Arends, R. Beck, G. Capitani, B. Dolbilkin, H. Falkenberg, G. Galler, S. Hall, J. Kellie, R. Kondratjev, R. Kordsmeier, V. Lisin, A. L’vov, G. Miller, C. Molinari, P. Ottonello, A. Reolon, M. Sanzone, M. Schmitz, M. Schneider, M. Schumacher, O. Selke, T. Walcher, F. Wissmann, S. Wolf, and A. Zucchiatti, *Nucl. Phys. A* **620**, 385 (1997).
- [21] J. P. Miller, E. J. Austin, E. C. Booth, K. P. Gall, E. K. McIntyre, and D. A. Whitehouse, *Nucl. Instrum. Methods Phys. Res. Sect. A* **270**, 431 (1988).
- [22] L. S. Myers, Ph.D. thesis, University of Illinois at Urbana-Champaign, Champaign, IL, USA (2010).
- [23] R. Brun and F. Rademakers, *Nucl. Instrum. Meth. Phys. Res. A* **389**, 81 (1997).
- [24] W. Verkerke and D. Kirkby, *Statistical Problems in Particle Physics, Astrophysics and Cosmology (PHYSTAT 05): Proceedings, Oxford, UK, September 12-15, 2005*, eConf **C0303241** (2003).
- [25] B. Gabioud, J.-C. Alder, C. Joseph, J.-F. Loude, N. Morel, A. Perrenoud, J.-P. Perroud, M. T. Tran, E. Winkelmann, W. Dahme, H. Panke, D. Renker, Č. Zupančič, G. Strassner, and P. Truöl, *Phys. Rev. Lett.* **42**, 1508 (1979).
- [26] V. L. Highland, M. Salomon, M. Hasinoff, E. Mazzucato, D. Measday, J.-M. Poutissou, and T. Suzuki, *Nucl. Phys. A* **365**, 333 (1981).
- [27] W. R. Gibbs, B. F. Gibson, and G. J. Stephenson, Jr., *Phys. Rev. C* **11**, 90 (1975).
- [28] G. F. de Téramond, *Phys. Rev. C* **16**, 1976 (1977).
- [29] W. R. Gibbs and B. F. Gibson, Private communication.
- [30] J. Allison, K. Amako, J. Apostolakis, P. Arce, M. Asai, T. Aso, E. Bagli, A. Bagulya, S. Banerjee, G. Barrand, and B. Beck, *Nucl. Instrum. Meth. Phys. Res. A* **835**, 186 (2016).
- [31] L. S. Myers, J. R. M. Annand, J. Brudvik, G. Feldman, K. G. Fissum, H. W. Grieffhammer, K. Hansen, S. S. Henshaw, L. Isaksson, R. Jebali, M. A. Kovash, M. Lundin, D. G. Middleton, A. M. Nathan, B. Schröder, and S. C. Stave, *Phys. Rev. C* **92**, 025203 (2015).
- [32] K. Kossert, M. Camen, F. Wissmann, J. Ahrens, J. R. M. Annand, H.-J. Arends, R. Beck, G. Caselotti, P. Grabmayr, O. Jahn, P. Jennewein, M. I. Levchuk, A. I. L’vov, J. C. McGeorge, A. Natter, V. Olmos de León, V. A. Petrun’kin, G. Rosner, M. Schumacher, B. Seitz,

- F. Smend, A. Thomas, W. Weihofen, and F. Zapadtko, Phys. Rev. Lett. **88**, 162301 (2002).
- [33] R. Al Jebali, Ph.D. thesis, The University Of Glasgow, Glasgow, UK (2013).
- [34] M. Lacombe, B. Loiseau, R. Mau, J. Côté, P. Pirés, and R. de Turreil, Phys. Lett. B **101**, 139 (1981).
- [35] W. J. Briscoe, I. I. Strakovsky, and R. L. Workman, Institute of Nuclear Studies of The George Washington University Database [SAID]; <http://gwdac.phys.gwu.edu>.
- [36] B Strandberg, Ph.D. thesis, University Of Glasgow, Glasgow, UK (2017).
- [37] V. Lensky, V. Baru, J. Haidenbauer, C. Hanhart, A. Kudryavtsev, and U. G. Meißner, Eur. Phys. J. A **26**, 107 (2005).
- [38] V. E. Tarasov, W. J. Briscoe, H. Gao, A. E. Kudryavtsev, and I. I. Strakovsky, Phys. Rev. C **84**, 035203 (2011).
- [39] M. I. Levchuk, A. Y. Loginov, A. A. Sidorov, V. N. Stibunov, and M. Schumacher, Phys. Rev. C **74**, 014004 (2006).
- [40] M. Döring, E. Oset, and M. J. Vicente Vacas, Phys. Rev. C **70**, 045203 (2004).
- [41] R. Machleidt, Phys. Rev. C **63**, 024001 (2001).
- [42] V. Bernard, N. Kaiser, and U.-G. Meißner, Phys. Lett. B **383**, 116 (1996).